6

Ultra Wideband (UWB) Pulse Reflection from a Dispersive Medium Half Space

Qingsheng Zeng[1] and Gilles Y. Delisle[2]
[1]*Communications Research Centre*
[2]*Technology Integration Centre, Technopôle Defense & Security*
Canada

1. Introduction

Electromagnetic wave reflection from dispersive media has been a subject of interest to researchers for many years. The advent of ultra wideband (UWB) short pulse sources has recently attracted renewed interest in this aspect. Accurate modeling and improved physical understanding of pulse reflection from dispersive media is crucial in a number of applications, including optical waveguides, UWB radar, ground penetrating radar, UWB biological effects, stealth technology and remote sensing. Numerous researchers have demonstrated that Lorentz, Debye and Cole-Cole models can be used to accurately predict dispersive properties of many media.

In the seminal work of Sommerfeld (Sommerfeld, 1914) and in the subsequent refinements of Oughstun and Sherman (Oughstun & Sherman, 1988) (Oughstun & Sherman, 1989) (Oughstun & Sherman, 1990), the investigations have focused on the Lorentz material, which is a good model for many materials encountered in optics and engineering. The reflection of a short pulse by a Lorentz medium has been considered for TE (transverse electric) polarization by Gray (Gray, 1980) and for TM (transverse magnetic) polarization by Stanic et al (Stanic et al., 1991). In each of these studies, the authors find the impulse response of the reflected field by calculating the inverse transform of the frequency domain reflection coefficient as an infinite series of fractional order Bessel functions. Although this gives a convenient analytical result, the series form provides little insight into the behavior of the reflected field waveform. Cossman et al have presented a compact form for both TE (Cossman et al., 2006) and TM (Cossman et al., 2007) reflection coefficients, which provide useful intuition about the response of a Lorentz medium half space. However, the mathematical derivations are lengthy and the solutions involve exponential and modified Bessel functions and require convolution operation to evaluate. Particularly, because of the greater complexity of the TM frequency domain reflection coefficient, a more involved process is needed, including the introduction of a term that does not appear in the TE case. Under some conditions this term is noncausal, although the final expression for the impulse response is causal. Moreover, when the incident angle is equal to 45^0, the general expressions cannot be used directly due to singularities, and a special form of TM time domain reflection coefficient is separately achieved.

The use of short pulses to probe materials has prompted the study of the reflection of transient waves from material half space of other types. The Debye model (Debye, 1945) is

utilized to describe the frequency behavior of the permittivity of many type materials, especially polar liquids. This model has been extended to include conductivity (Kosmas et al., 2004) and several relaxation components (Oswald et al., 1998), and has been used to describe the behavior of such diverse materials as biological tissues (Ong et al., 2003), building materials (Ogunsola et al., 2006), circuit boards (Zhang et al., 2003) and ceramics (Guerra & Eiras, 2004). A standard technique for the measurement of material parameters is to interrogate the material, either in free space (Piesiewicz et al., 2005) or in a waveguide system (Jones et al., 2005) with an electromagnetic pulse. It is therefore important to have an efficient method analyzing the time-domain reflection properties of a Debye material. Rothwell (Rothwell, 2007) worked out the time domain reflection coefficients of a Debye half space for both horizontal and vertical polarizations that involve exponential and modified Bessel functions and require convolution operations to evaluate. Another model commonly used to capture the relaxation-based dispersive properties is the Cole–Cole model (Cole & Cole, 1941) that is more general than the Debye model. For many types of materials including biological tissues, the Cole–Cole models provided an excellent fit to experimental data over the entire measurement frequency range. However, to our knowledge, the time-domain reflection coefficient of a Cole–Cole half space for any polarization has been not available so far, perhaps due to the computational complexity of embedding a Cole–Cole dispersion model into numerical methods.

All materials are to some extent dispersive. If a field applied to a material undergoes a sufficient rapid change, there is a time lag in the response of the polarization or magnetization of the atoms. It has been found that such materials have complex, frequency dependent constitutive parameters. On the one hand, the lossy material is dispersive since it has a complex, frequency dependent permittivity. On the other hand, the Kronig−Kramers relations imply that if the constitutive parameters of a material are frequency dependent, they must have both real and imaginary parts (Rothwell & Cloud, 2001). Such a material, if isotropic, must be lossy. So dispersive materials are general lossy and must have both dissipative and energy storage characteristics. However, many materials have frequency range called transparency ranges over which the imaginary parts are smaller compared to real parts of constitutive parameters. If we restrict our interest to these ranges, we may approximate the material as lossless.

In this chapter, the time domain technique based on the numerical inversion of Laplace transform is developed and extended to the modeling of ultra wideband pulse reflection from Lorentz, Debye and Cole−Cole media. All these three dispersive models satisfy the Kronig−Kramers relations required for a causal material (Rothwell & Cloud, 2001). Firstly, for readers' convenience, the numerical inversion of Laplace transform is presented. Next, the time domain reflection coefficients, viz impulse responses, of Lorentz, Debye and Cole−Cole half spaces are achieved for both TE and TM cases. Then, the transient reflections of an arbitray pulse from these media are determined by convolving the incident pulse with the impulse responses of these media, instead of using Prony's method to decompose the incident pulse into a series of finite attenuating exponential signals as in our previous work (Zeng & Delisle, 2006). Based on the time domain analysis of reflected pulses from these dispersive half spaces, some waveform parameters are estimated and the material diagnosis is carried out. Lastly, the work on transient wave reflection from dispersive media is summarized with some meaningful conclusions. Our results show excellent agreement with those in the literature, validating the correctness and effectiveness of our technique.

2. Numerical inversion of Laplace transform

The Laplace transform (image function in the complex frequency domain) $F(s)$ and the inverse Laplace transform (original function in the time domain) $f(t)$ are related by the forward transformation

$$Lf(t) = F(s) = \int_0^\infty f(t) e^{-st} dt \tag{1}$$

and the inverse transformation

$$L^{-1}F(s) = f(t) = \frac{1}{2\pi j}\int_{\gamma-j\infty}^{\gamma+j\infty} F(s) e^{st} ds\,. \tag{2}$$

In general, it is straightforward to take the Laplace transform of a function. However, the inverse transformation is often difficult. In many cases, the method using simple rules and a table of transforms, and the method using the Bromwich integral and Cauchy integral theorem do not work well, hence some numerical technique must be utilized. To implement the numerical inversion method, the following conditions must be satisfied (Zeng, 2010). Based on the properties of $F(s)$, such a number γ_0 can always be found that in the region of convergence, $0 < \gamma_0 < \mathrm{Re}(s)$, 1) $F(s)$ converges absolutely, 2) $\lim_{s\to\infty} F(s) = 0$, 3) $F(s)$ does not have any singularity and branch point, and 4) $F(s^*) = F^*(s)$ where the asterisk denotes complex conjugate.

The most distinctive feature of this method lies in the approximation for e^{st}. Its main points are:

i) $$e^{st} = \lim_{\rho\to\infty} \frac{e^{\rho}}{2\cosh(\rho - st)} = e^{st} - e^{-2\rho} e^{3st} + e^{-4\rho} e^{5st} - \cdots \tag{3}$$

ii) $$e^{st} \approx E_{ec}(st,\rho) = \frac{e^{\rho}}{2\cosh(\rho - st)} = \frac{e^{\rho}}{2}\sum_{n=-\infty}^{\infty} \frac{(-1)^n j}{st - [\rho + j(n-0.5)\pi]} \tag{4}$$

iii) The Bromwich integral is transformed to the integral around the poles of $E_{ec}(st,\rho)$.

Then $f(t)$ is approximated by $f_{ec}(t,\rho)$, which is expressed by

$$f_{ec}(t,\rho) = \frac{1}{2\pi j}\int_{\gamma-j\infty}^{\gamma+j\infty} F(s) E_{ec}(st,\rho)\, ds = f(t) - e^{-2\rho} f(3t) + e^{-4\rho} f(5t) - \cdots = (e^{\rho}/t)\sum_{n=1}^{\infty} F_n \tag{5}$$

where $t > 0$, and

$$F_n = (-1)^n \,\mathrm{Im}\, F\{[\rho + j(n-0.5)\pi]/t\} \tag{6}$$

Equation (5) shows that the function $f_{ec}(t,\rho)$ gives a good approximation to $f(t)$ when $\rho >> 1$, and can be used for error estimation. Equations (5) and (6) are derived by substituting $E_{ec}(st,\rho)$ from (4), and can be applied to the numerical inversion of the Laplace transform. In practice, the infinite series in (5) has to be truncated after a proper number of

terms. Since the infinite series is a slowly convergent alternating series, truncating to a small number of terms leads to a significant error. An effective approach using the Euler transformation has been developed, which works under the following conditions (Hosono, 1981): a) There exists an integer $k \geq 1$ such that the signs of F_n alternate for $n \geq k$; b) For $n \geq k$, $\frac{1}{2} < \left| F_{n+1} / F_n \right| \leq 1$. With conditions a) and b), (5) can be truncated with $f_{ec}^{lm}(t,a)$, which has $N = l + m$ terms and is given by

$$f_{ec}^{lm}(t,\rho) = \left(e^{\rho}/t\right)\left(\sum_{n=1}^{l-1} F_n + 2^{-m-1}\sum_{n=0}^{m} A_{mn} F_{l+n}\right) \tag{7}$$

where A_{mn} are defined recursively by

$$A_{mm} = 1, \quad A_{mn-1} = A_{mn} + \binom{m+1}{n}. \tag{8}$$

In this method, the upper bound for the truncation errors is given by

$$R^{lm} = \left| f_{ec}^{l+1,m}(t,\rho) - f_{ec}^{l,m}(t,\rho) \right| \tag{9}$$

while the upper bound for the approximation errors is given by

$$\left| f_{ec}(t,\rho) - f(t) \right| \approx M e^{-2\rho}, \tag{10}$$

If

$$\left| f(t) \right| \leq M \qquad \text{for all} \qquad t > 0 .$$

As indicated in (10), the relative approximation errors are less than $e^{-2\rho}$, while the truncation errors increase with t and decrease with N. For a typical value of t, the calculation is repeated by increasing N to determine a proper number of terms in (5), which makes the truncation errors small enough.

3. Pulse reflection from a Lorentz medium half space

Consider a sinusoidal stead-state plane wave of frequency ω incident on an interface separating free space (region 1) from a homogeneous Lorentz medium (region 2). The angle of incidence measured from the normal to the interface is θ, and the electric field is polarized perpendicular to the plane of incidence (TE polarization). Region 1 is described by the permittivity ε_0 and permeability μ_0, while region 2 is described by the permittivity $\varepsilon(\omega) = \varepsilon_0 \varepsilon_r(\omega)$ and permeability μ_0. The reflection coefficient, defined as the ratio of the tangential incident field to reflected electric field, is given by (Cossman et al., 2006)

$$\Gamma(\omega) = \frac{Z(\omega) - Z_0}{Z(\omega) + Z_0}, \tag{11}$$

where the wave impedance of the incident wave is $Z_0 = \eta_0 / \cos\theta$ and the wave impedance of the transmitted wave is

$$Z(\omega)=\frac{\eta(\omega)\,k(\omega)}{k_z(\omega)}. \tag{12}$$

Here $\eta_0=(\mu_0/\varepsilon_0)^{1/2}$, $\eta=(\mu_0/\varepsilon)^{1/2}$, $k_z=\left(k^2-k_0^2\sin^2\theta\right)^{1/2}$, $k_0=\omega(\mu_0\varepsilon_0)^{1/2}$ and $k=\omega(\mu_0\varepsilon)^{1/2}$. The relative permittivity of a single resonance Lorentz medium has the form

$$\varepsilon_r(\omega)=1+\frac{b^2}{\omega_0^2-\omega^2+2j\omega\delta}. \tag{13}$$

Here ω_0 is the resonance frequency, δ is the damping coefficient, and b is the plasma frequency of the medium. Letting the Laplace transform variable be $s=j\omega$ and substituting Equation (13), then the Laplace domain reflection coefficient may be written in the form

$$\Gamma(s)=\frac{\left(s^2+2\delta s+\omega_0^2\right)^{1/2}-\left(s^2+2\delta s+\omega_0^2+B^2\right)^{1/2}}{\left(s^2+2\delta s+\omega_0^2\right)^{1/2}+\left(s^2+2\delta s+\omega_0^2+B^2\right)^{1/2}} \tag{14}$$

where $B=b/\cos\theta$. Factoring the quadratic forms under the radicals gives the alternative form

$$\Gamma(s)=\frac{\left((s-s_1)(s-s_2)\right)^{1/2}-\left((s-s_3)(s-s_4)\right)^{1/2}}{\left((s-s_1)(s-s_2)\right)^{1/2}+\left((s-s_3)(s-s_4)\right)^{1/2}} \tag{15}$$

where

$$s_{1,2}=-\delta\pm\lambda_1 \qquad \lambda_1=\left(\delta^2-\omega_0^2\right)^{1/2}, \tag{16}$$

$$s_{3,4}=-\delta\pm\lambda_3 \qquad \lambda_3=\left(\delta^2-\omega_0^2-B^2\right)^{1/2}, \tag{17}$$

λ_1 and λ_3 may be either real or imaginary, depending on the values of ω_0, δ and B. The image function $\Gamma(s)$ given in (15) clearly satisfies four conditions 1) – 4) listed in Section 2 under which $f(t)$ can be approximated by $f_{ec}(t,\rho)$. It can be proved that, for $s=\left[\rho+j(n-0.5)\pi\right]/t$, $\Gamma(s)$ meets both two conditions a) and b) described in Section 2 under which $f_{ec}^{lm}(t,\rho)$ can be used to approximate $f_{ec}(t,\rho)$ (Zeng, 2010). The proof would not be given here due to the limited space. So the transient reflection coefficient $\Gamma(t)$, the original function of $\Gamma(s)$, can be calculated using Equation (7).

To compare our results with those in (Cossman et al, 2006), the same incident angle, $\theta=30^0$, and the same three sets of parameters are chosen as in (Cossman et al., 2006), with each set of parameters corresponding to each of the three possible cases. The first set of parameters is chosen as $\omega_0=4.0\times10^{16}\,s^{-1}$, $\delta=0.28\times10^{16}\,s^{-1}$, $b^2=20.0\times10^{32}\,s^{-2}$, corresponding to case 1 for $\delta<<\omega_0$. In this case, the waveform highly oscillates and only slightly damps, as plotted in Figure 1 (a).

The next set of parameters is $\omega_0=2.0\times10^{15}\,s^{-1}$, $\delta=0.28\times10^{16}\,s^{-1}$, $b^2=20.0\times10^{29}\,s^{-2}$. This choice of parameter corresponds to case 2 for $\delta^2>\omega_0^2+B^2$, where the resulting waveform is overdamped and has only one single negative peak without any oscillation, as shown in Figure 1 (b).

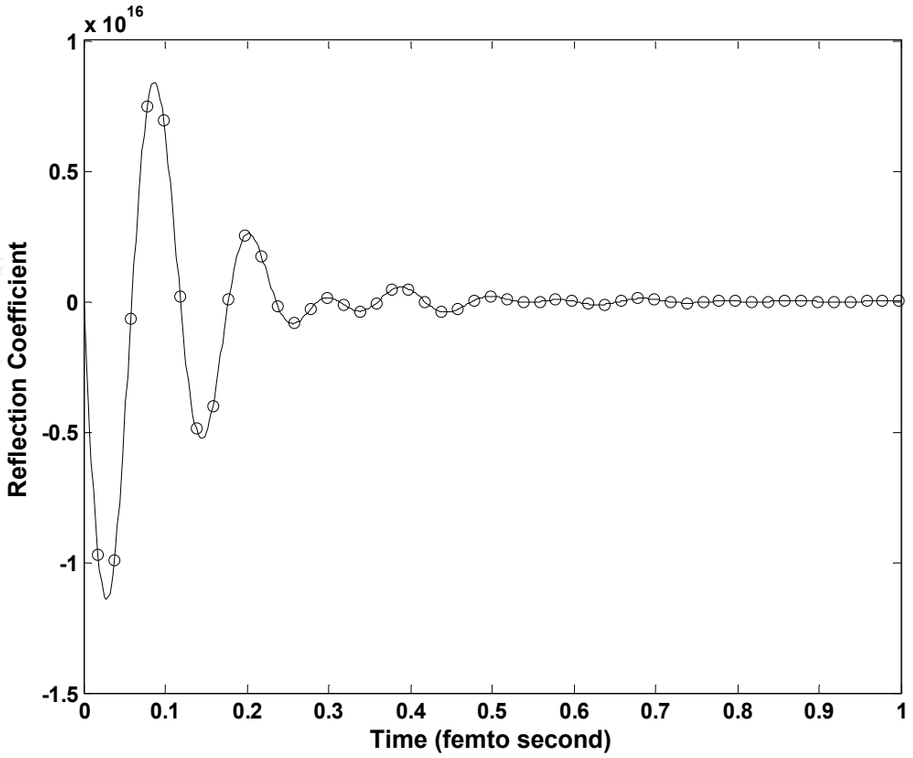

(a) $\omega_0 = 4.0 \times 10^{16} s^{-1}$, $\delta = 0.28 \times 10^{16} s^{-1}$, $b^2 = 20.0 \times 10^{32} s^{-2}$, $\delta << \omega_0$.

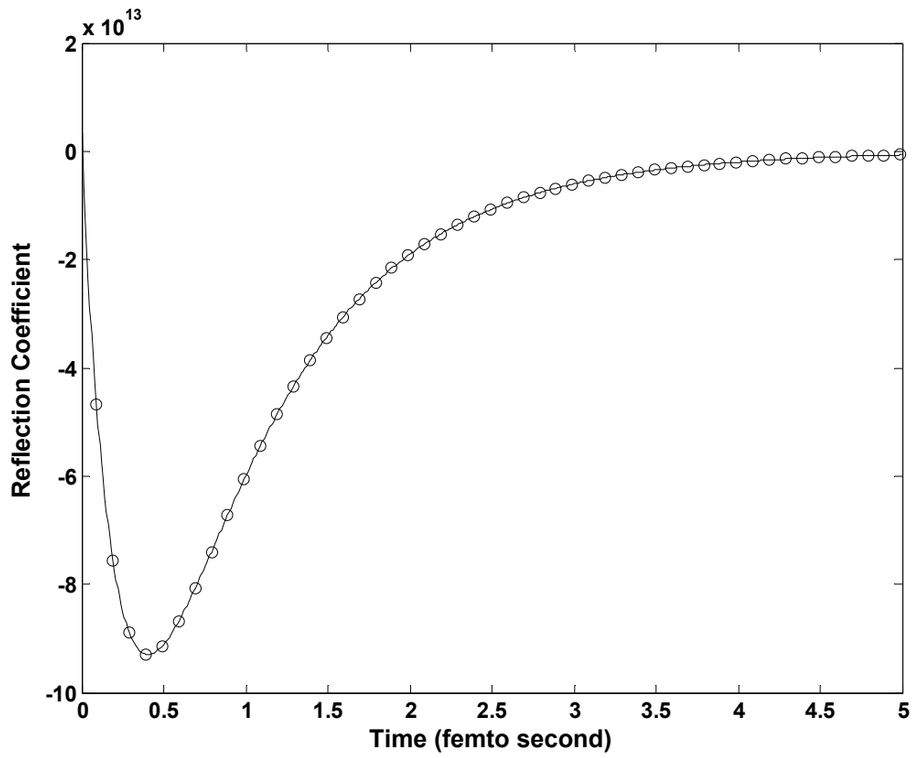

(b) $\omega_0 = 2.0 \times 10^{15} s^{-1}$, $\delta = 0.28 \times 10^{16} s^{-1}$, $b^2 = 20.0 \times 10^{29} s^{-2}$, $\delta^2 > \omega_0^2 + B^2$

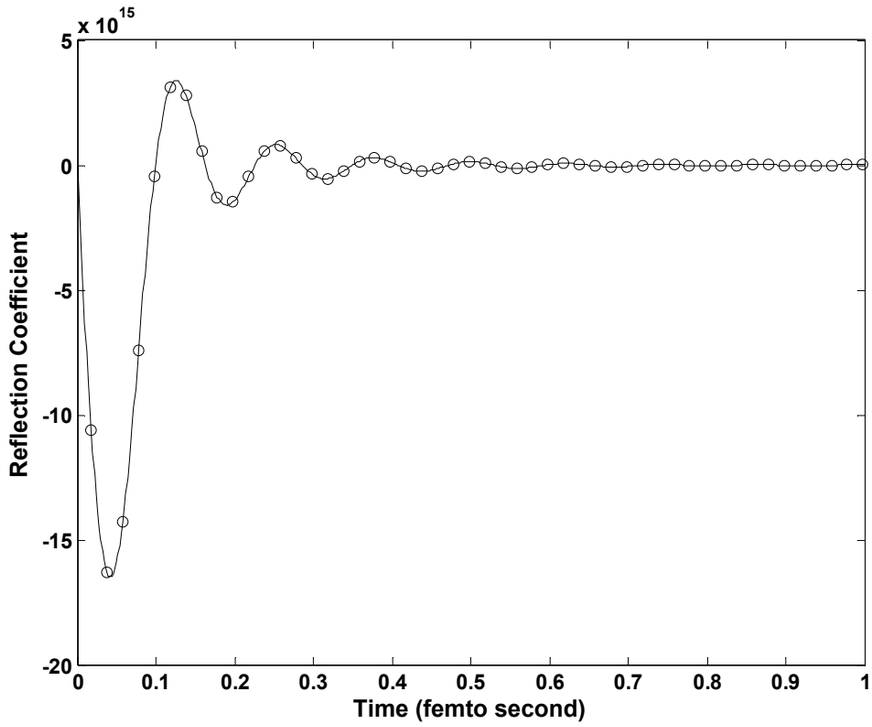

(c) $\omega_0 = 2.0\times10^{15}s^{-1}$, $\delta = 0.28\times10^{16}s^{-1}$, $b^2 = 20.0\times10^{32}s^{-2}$, $\delta > \omega_0$ but $\delta^2 < \omega_0^2 + B^2$.

Fig. 1. Transient reflection coefficient for TE polarization with incident angle $\theta = 30^0$ and three sets of material parameters. Solid line – our result; Small circle – result in (Cossman et al., 2006).

The third choice of parameters is $\omega_0 = 2.0\times10^{15}s^{-1}$, $\delta = 0.28\times10^{16}s^{-1}$, $b^2 = 20.0\times10^{32}s^{-2}$, which corresponds to case 3 for $\delta > \omega_0$ but $\delta^2 < \omega_0^2 + B^2$. In this case, the waveform has more damping and less oscillation than that in case 1, but has more oscillation than that in case 2, as illustrated in Figure 1 (c).

For the case of TM polarization (magnetic field perpendicular to the plane of incidence), the originally defined reflection coefficient is still given by (11), the impedance of a plane wave in the free space (ratio of tangential electric field to tangential magnetic field at the interface) is $Z_0 = \eta_0 \cos\theta$, the impedance of a wave in the Lorentz medium is

$$Z(\omega) = \frac{\eta(\omega)\, k_z(\omega)}{k(\omega)}. \tag{18}$$

The incident angle θ is measured in the same way as in TE case, η_0, η, k_z, k_0, and k are the same as those for TE polarization, respectively. Letting the Laplace transform variable be $s = j\omega$ and substituting (13) and (18) into (11), the Laplace domain reflection coefficient may be written in the form

$$\Gamma(s) = \frac{\left((s-s_1)(s-s_2)(s-s_5)(s-s_6)\right)^{1/2} - \left((s-s_3)(s-s_4)\right)^{1/2}}{\left((s-s_1)(s-s_2)(s-s_5)(s-s_6)\right)^{1/2} + \left((s-s_3)(s-s_4)\right)^{1/2}} = \frac{N(s)}{D(s)}, \tag{19}$$

where

$$s_{1,2} = -\delta \pm \lambda_1 \qquad \lambda_1 = \left(\delta^2 - \omega_0^2\right)^{1/2}, \tag{20}$$

$$s_{3,4} = -\delta \pm \lambda_3 \qquad \lambda_3 = \left(\delta^2 - \omega_0^2 - b^2\right)^{1/2}, \tag{21}$$

$$s_{5,6} = -\delta \pm \lambda_5 \qquad \lambda_5 = \left(\delta^2 - \omega_0^2 - B^2\right)^{1/2}. \tag{22}$$

Here ω_0, δ, b and B are the same as those for TE polarization, and λ_1, λ_3 and λ_5 may be either real or imaginary, depending on the values of ω_0, δ, b and B.

As indicated in the introduction, the solution of transient reflection coefficient in TM case is more complicated and involved than that in TE case. In (Cossman et al., 2007), a term that does not appear in the TE case needs to be introduced and a special form of the time domain reflection coefficient needs to be separately solved when the incident angle is equal to 45^0, which is however not needed with numerical Laplace transform. The image function $\Gamma(s)$ given in (19) obviously satisfies four conditions 1) – 4) listed in Section 2. Furthermore, it can also be proved that $\Gamma(s)$ given in (19) meets both two conditions a) and b) in Section 2 (Zeng, 2010).

To compare our results with those in (Cossman et al, 2007), the same incident angles and the same sets of material parameters are chosen as in (Cossman et al., 2007). The first case uses $\theta = 30^0$ along with the material parameters, $\omega_0 = 4.0 \times 10^{16} s^{-1}$, $\delta = 0.28 \times 10^{16} s^{-1}$, and $b^2 = 20.0 \times 10^{32} s^{-2}$, corresponding to the case for $\delta << \omega_0$. So the waveform of $\Gamma(t)$ is highly oscillatory and only slightly damped, as plotted in Figure 2 (a).

In the second case, the material parameters are chosen as $\omega_0 = 2.0 \times 10^{15} s^{-1}$, $\delta = 0.28 \times 10^{16} s^{-1}$, and $b^2 = 20.0 \times 10^{29} s^{-2}$, along with $\theta = 30^0$. This corresponds to the case for $\delta^2 > \omega_0^2 + B^2$, and the waveform of $\Gamma(t)$ shows no oscillatory behavior and only a single negative peak, as shown in Figure 2 (b).

In the third case, the choice of parameters is $\omega_0 = 2.0 \times 10^{15} s^{-1}$, $\delta = 0.28 \times 10^{16} s^{-1}$, $b^2 = 20.0 \times 10^{32} s^{-2}$, again with $\theta = 30^0$, which corresponds to the case for $\delta > \omega_0$ but $\delta^2 < \omega_0^2 + B^2$. Thus, $\Gamma(t)$ is more damping and less oscillatory than with the first choice of parameters but more oscillatory than with the second choice of parameters, as illustrated in Figure 2 (c).

In the fourth case, the material parameters are the same as those in the first case, but $\theta = 50^0$ is used. The result is achieved by directly using our approach that does not lead to any noncasual term, and is plotted in Figure 2 (d).

The final case examines the special case of $\theta = 45^0$ with the same choice of material parameters as in the first case. With our approach, this case does not need to be processed separately and can be treated as a general case for any incident angle. This result is illustrated in Figure 2 (e), and is very similar to that shown in Figure 2 (d), since the incident angle in this case differs by only 5^0 from that in the fourth case.

Figure 1 and Figure 2 demonstrate that our results perfectly agree with those in (Cossman et al., 2006) and in (Cossman et al., 2007), respectively, for all the different cases.

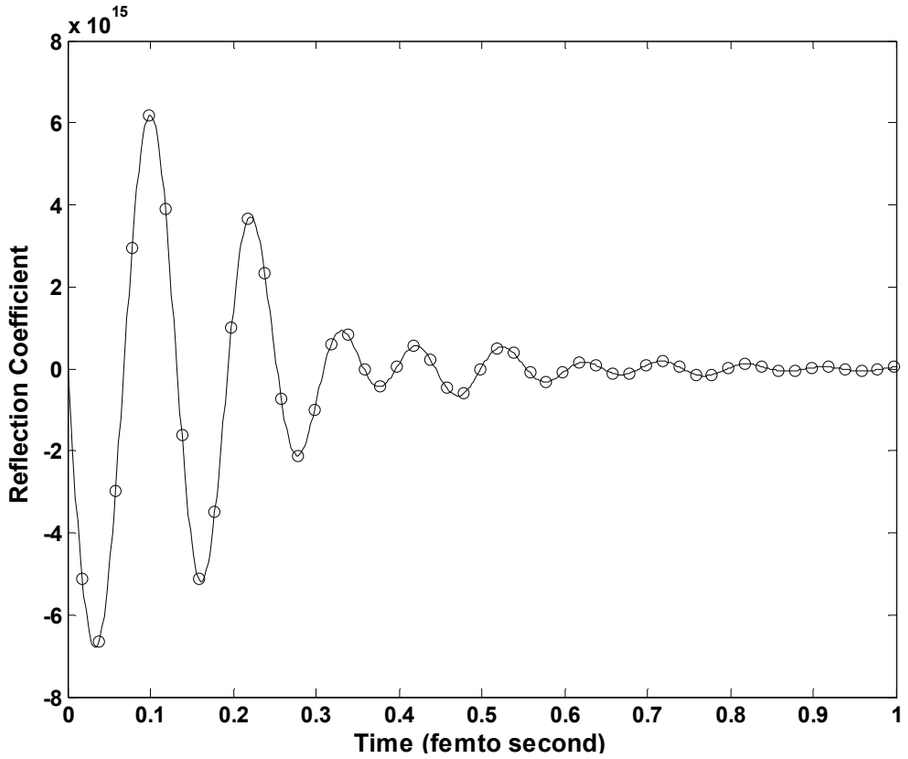

(a) $\theta = 30^0$, $\omega_0 = 4.0 \times 10^{16} s^{-1}$, $\delta = 0.28 \times 10^{16} s^{-1}$, $b^2 = 20.0 \times 10^{32} s^{-2}$, $\delta << \omega_0$.

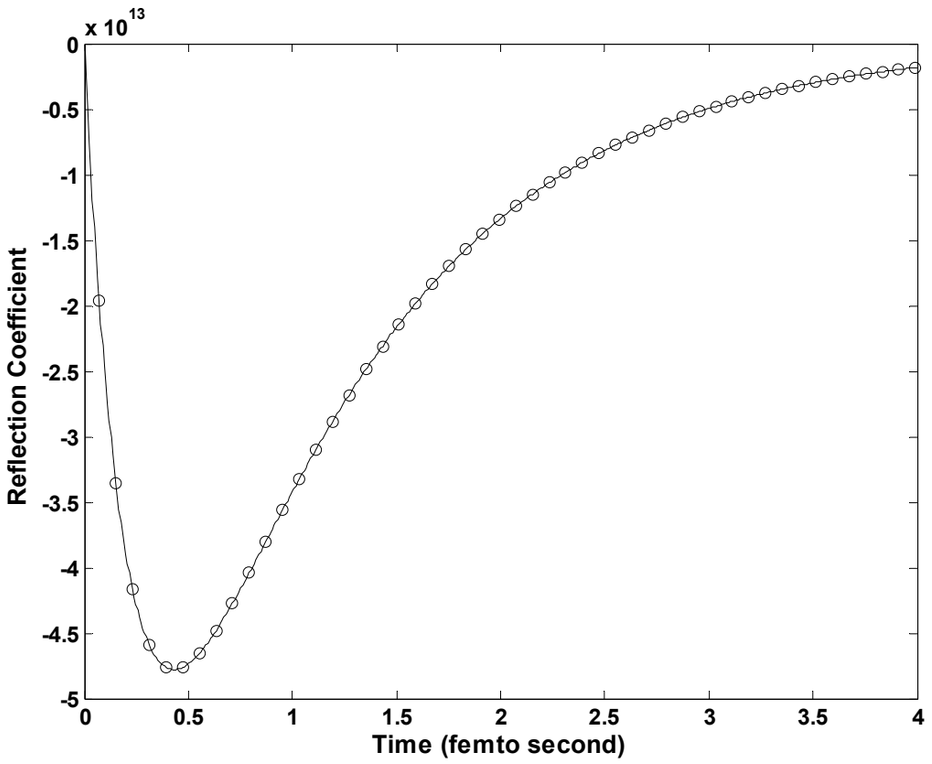

(b) $\theta = 30^0$, $\omega_0 = 2.0 \times 10^{15} s^{-1}$, $\delta = 0.28 \times 10^{16} s^{-1}$, $b^2 = 20.0 \times 10^{29} s^{-2}$, $\delta^2 > \omega_0^2 + B^2$.

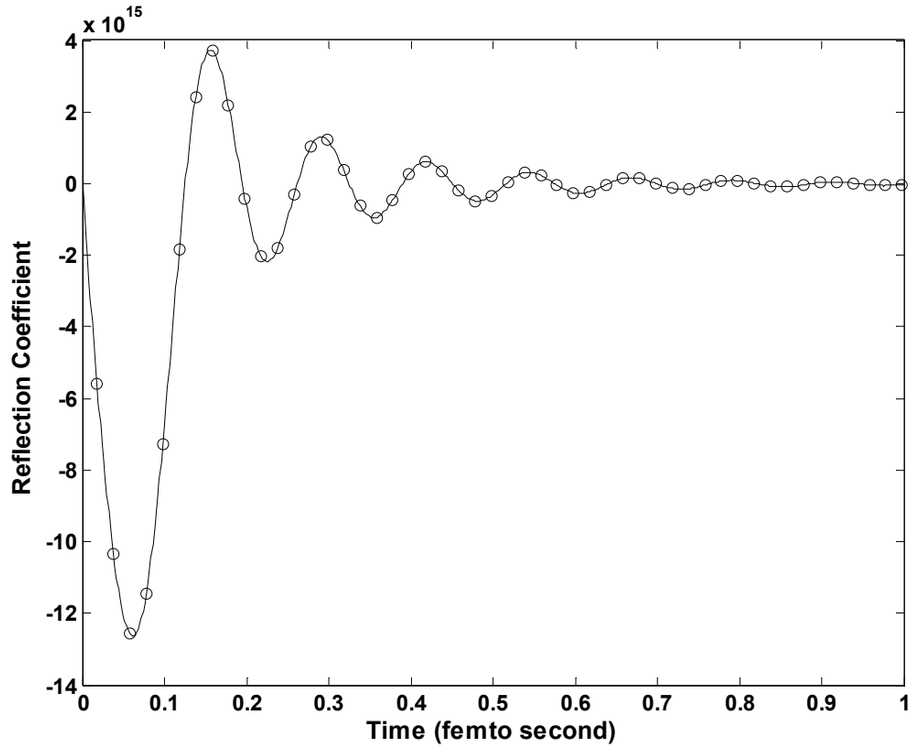

(c) $\theta = 30^0$, $\omega_0 = 2.0 \times 10^{15} s^{-1}$, $\delta = 0.28 \times 10^{16} s^{-1}$, $b^2 = 20.0 \times 10^{32} s^{-2}$, $\delta > \omega_0$ but $\delta^2 < \omega_0^2 + B^2$.

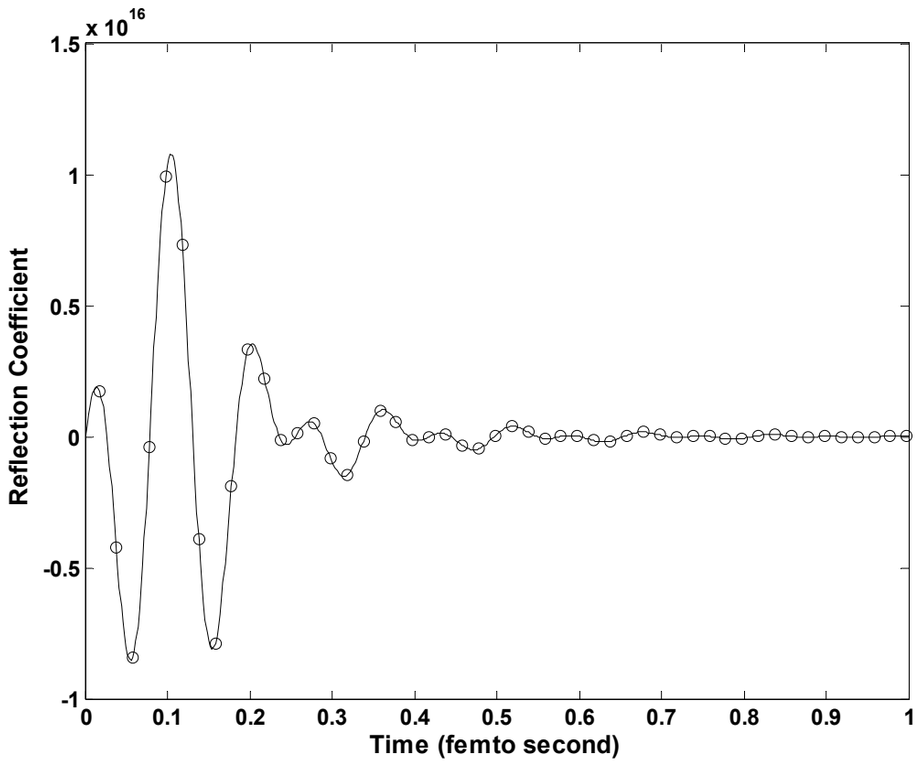

(d) $\theta = 50^0$, $\omega_0 = 4.0 \times 10^{16} s^{-1}$, $\delta = 0.28 \times 10^{16} s^{-1}$, $b^2 = 20.0 \times 10^{32} s^{-2}$, $\delta << \omega_0$.

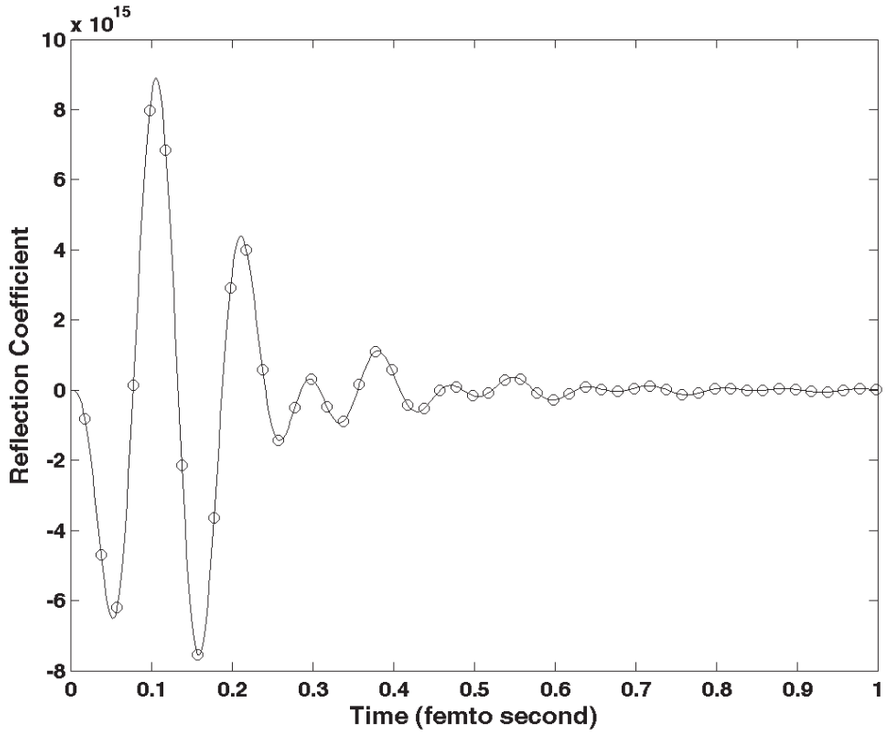

(e) $\theta = 45^0$, $\omega_0 = 4.0 \times 10^{16} s^{-1}$, $\delta = 0.28 \times 10^{16} s^{-1}$, $b^2 = 20.0 \times 10^{32} s^{-2}$, $\delta << \omega_0$.

Fig. 2. Transient reflection coefficient for TM polarization, with incident angle $\theta = 30^0$ and three sets of material parameters (a) (b) (c), and with incident angle $\theta = 50^0$ and $\theta = 45^0$ and one set of material parameters (d) (e) . Solid line – our result; Small circle – result in (Cossman et al., 2007).

4. Pulse reflection from a Debye and Cole–Cole medium half space

The knowledge of material properties is required in various technological fields, such as geophysics, material science and biomedical engineering. The characterization of bulk materials would be the most direct way to acquire this knowledge and greatly helpful to understand the underlying physics at the microscopic level, which is much more complicated in comparison with the existing formulations of the bulk effects. A typical approach to bulk material characterization is to examine reflected electromagnetic pulses from the interface between free space and the investigated material. Many kinds of materials show the relaxation-based dispersive properties that are commonly captured by the Debye (Debye, 1945) and Cole–Cole (Cole & Cole, 1941) models. Rothwell (Rothwell, 2007) worked out the time domain reflection coefficients of a Debye half space for both horizontal and vertical polarizations that involve exponential and modified Bessel functions and require convolution operations to evaluate. To our knowledge, the time domain reflection coefficient of a Cole–Cole half space for any polarization has been not available so far. It is the purpose of this section to develop a new technique for transient analysis of pulse reflection from Debye and Cole–Cole media, and apply this technique to waveform parameter estimation and material characterization.

4.1 Time domain reflection coefficients

Without losing generality and for the comparison with the results in (Rothwell, 2007), the one-order model with zero ionic conductivity is utilized in this work. Introduce the Laplace variable $s = j\omega$, and consider the interface between free space and a dielectric half space with unity permeability and a permittivity $\varepsilon(s) = \varepsilon_0 \varepsilon_r(s)$ described by the following unified equation

$$\varepsilon_r(s) = \varepsilon_\infty + \frac{\varepsilon_s - \varepsilon_\infty}{1 + (s\tau)^{1-\alpha}}, \tag{23}$$

where ε_s and ε_∞ are the static and optical dielectric constants ($\varepsilon_s > \varepsilon_\infty$), respectively, τ is the relaxation time, (23) becomes a one-pole Debye equation when $\alpha = 0$, and is a one-order Cole–Cole equation when $0 < \alpha \le 1$. A nonzero Cole–Cole parameter α is a measure for broadening dispersion, which tends to broaden the relaxation spectrum and results from a spread of relaxation times centered around τ (Rothwell & Cloud, 2001). A unified formulation for a Cole–Cole or Debye half space is given below.

A plane wave is obliquely incident onto a dispersive half space from free space, at an incidence angle θ relative to the normal to the interface. The reflection coefficients are given by

$$R_H(s) = \frac{\cos\theta - \sqrt{\varepsilon_r(s) - \sin^2\theta}}{\cos\theta + \sqrt{\varepsilon_r(s) - \sin^2\theta}} \tag{24}$$

and

$$R_V(s) = \frac{\sqrt{\varepsilon_r(s) - \sin^2\theta} - \varepsilon_r(s)\cos\theta}{\sqrt{\varepsilon_r(s) - \sin^2\theta} + \varepsilon_r(s)\cos\theta} \tag{25}$$

for horizontal and vertical polarizations, respectively. Substituting $\varepsilon_r(s)$ from (23) leads to

$$R_H(s) = \frac{\sqrt{s^{1-\alpha} + s_0} - K_H\sqrt{s^{1-\alpha} + s_1}}{\sqrt{s^{1-\alpha} + s_0} + K_H\sqrt{s^{1-\alpha} + s_1}} \tag{26}$$

and

$$R_V(s) = \frac{\sqrt{s^{1-\alpha} + s_0}\sqrt{s^{1-\alpha} + s_1} - K_V\left(s^{1-\alpha} + s_2\right)}{\sqrt{s^{1-\alpha} + s_0}\sqrt{s^{1-\alpha} + s_1} + K_V\left(s^{1-\alpha} + s_2\right)}, \tag{27}$$

where

$$s_0 = \left(\frac{1}{\tau}\right)^{1-\alpha},\ s_1 = \left(\frac{1}{\tau}\right)^{1-\alpha}\frac{\varepsilon_s - \sin^2\theta}{\varepsilon_\infty - \sin^2\theta} > s_0,\ s_2 = \left(\frac{1}{\tau}\right)^{1-\alpha}\frac{\varepsilon_s}{\varepsilon_\infty}, \tag{28}$$

$$K_H = \frac{\sqrt{\varepsilon_\infty - \sin^2\theta}}{\cos\theta}, \tag{29}$$

and

$$K_V = \frac{\varepsilon_\infty \cos\theta}{\sqrt{\varepsilon_\infty - \sin^2\theta}}. \tag{30}$$

Either $R_H(s)$ or $R_V(s)$ does not satisfy the second one of the four conditions listed in Section 2, that is, is not asymptotic to zero at high frequency, but instead

$$\lim_{s\to\infty} R_H(s) = R_H^\infty = \frac{1-K_H}{1+K_H}, \tag{31}$$

and

$$\lim_{s\to\infty} R_V(s) = R_V^\infty = \frac{1-K_V}{1+K_V}. \tag{32}$$

So $R_H(t)$ and $R_V(t)$ have the impulsive components, $R_H^\infty(t)$ and $R_V^\infty(t)$, with the amplitudes of R_H^∞ and R_V^∞, respectively. Subtracting the terms R_H^∞ and R_V^∞ from $R_H(s)$ and $R_V(s)$ respectively gives the "reduced" reflection coefficients,

$$\bar{R}_H(s) = R_H(s) - R_H^\infty = \frac{2K_H}{1+K_H} \frac{\sqrt{s^{1-\alpha}+s_0} - \sqrt{s^{1-\alpha}+s_1}}{\sqrt{s^{1-\alpha}+s_0} + K_H\sqrt{s^{1-\alpha}+s_1}}, \tag{33}$$

and

$$\bar{R}_V(s) = R_V(s) - R_V^\infty = \frac{2K_V}{1+K_V} \frac{\sqrt{s^{1-\alpha}+s_0}\sqrt{s^{1-\alpha}+s_1} - \left(s^{1-\alpha}+s_2\right)}{\sqrt{s^{1-\alpha}+s_0}\sqrt{s^{1-\alpha}+s_1} + K_V\left(s^{1-\alpha}+s_2\right)}. \tag{34}$$

Both $\bar{R}_H(s)$ and $\bar{R}_V(s)$ satisfy the four conditions in Section 2, under which $f(t)$ can be approximated by $f_{ec}(t,\rho)$. It can be proved that, for $s = \left[\rho + j(n-0.5)\pi\right]/t$, both $\bar{R}_H(s)$ and $\bar{R}_V(s)$ also obey the two conditions a) and b) in Section 2, under which $f_{ec}^{lm}(t,\rho)$ can be used to approximate $f_{ec}(t,\rho)$ (Zeng, 2010). Hence, both reduced time domain reflection coefficients $\bar{R}_H(t)$ and $\bar{R}_V(t)$ can be calculated using Equation (7). The required time domain reflection coefficients $R_H(t)$ and $R_V(t)$ are obtained by adding $R_H^\infty(t)$ and $R_V^\infty(t)$ to $\bar{R}_H(t)$ and $\bar{R}_V(t)$, respectively.

Before applying this technique to waveform parameter estimation and material characterization, its correctness and effectiveness are verified by comparing the reduced transient reflection coefficients with those in (Rothwell, 2007). Several different cases are considered, each following the Debye model ($\alpha = 0$) with different values of the parameters ε_s, ε_∞ and τ. In the numerical trials, for each ρ value (ρ = 3, 6, 10 and 20), we set N = 15 (l = 9, m = 6), 20 (l = 14, m = 6), 39 (l = 20, m = 19), 59 (l = 29, m = 30), and 99 (l = 49, m = 50) and achieved almost the same results for $f_{ec}^{lm}(t,\rho)$, indicating that the truncation errors are small enough. In the following examples, ρ = 3 and N = 15 (l = 9, m = 6).

Figure 3 (a) illustrates the reduced reflection coefficients of water (at standard temperature and pressure) calculated using our technique, and compares them to the results in (Rothwell, 2007) with an excellent agreement. The reduced reflection coefficients do not

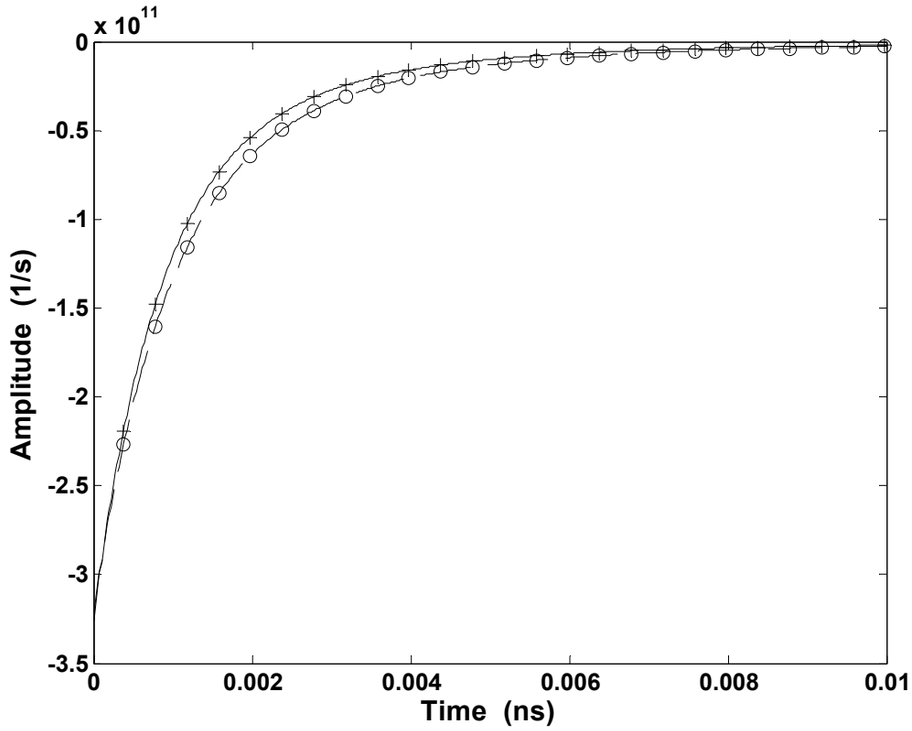

(a) Water, $\alpha = 0$, $\varepsilon_s = 78.3$, $\varepsilon_\infty = 5.0$, $\tau = 9.6 \times 10^{-12}$ s.

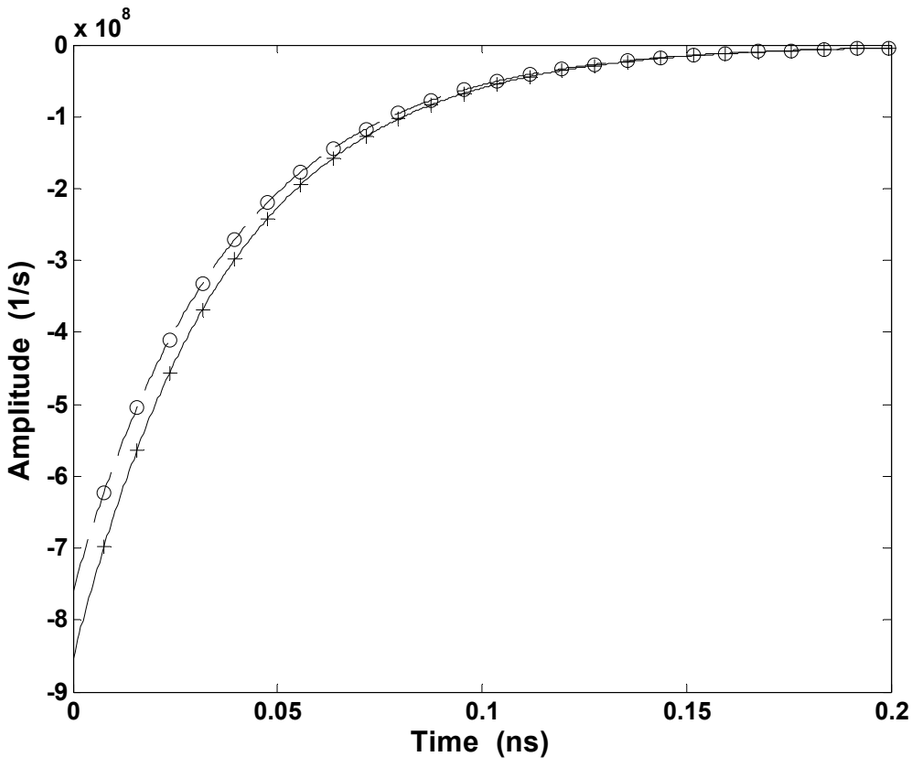

(b) Martian soil simulant, $\alpha = 0$, $\varepsilon_s = 3.57$, $\varepsilon_\infty = 3.12$, $\tau = 0.041 \times 10^{-9}$ s.

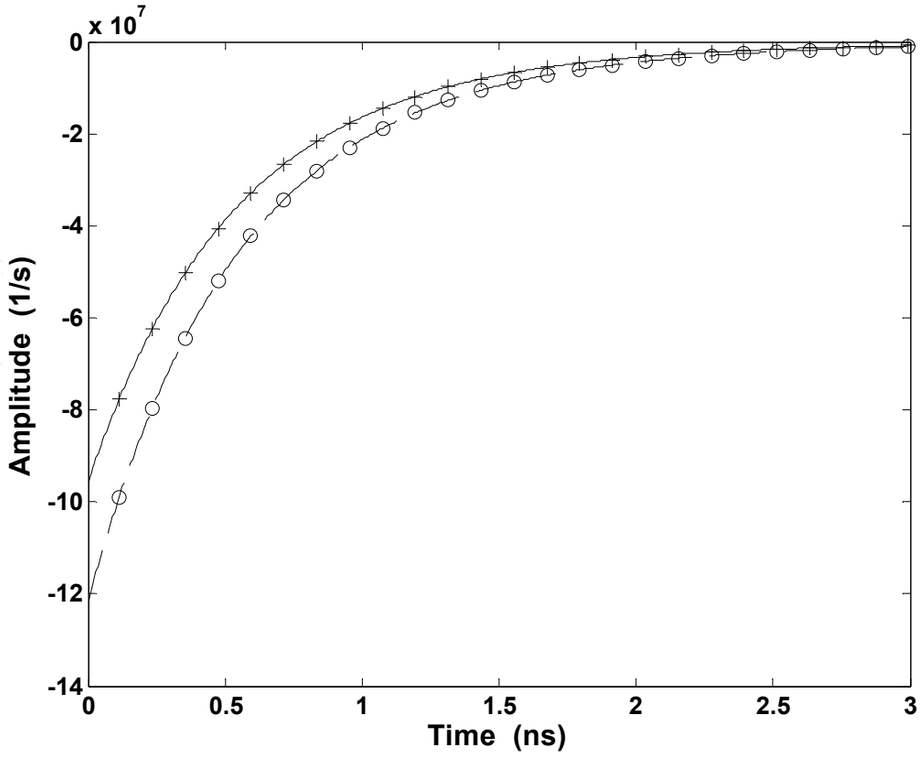

(c) Ceramic, $\alpha = 0$, $\varepsilon_s = 494$, $\varepsilon_\infty = 155$, $\tau = 1.39 \times 10^{-9}$ s.

Fig. 3. Time domain reduced reflection coefficients of Debye half space for $\theta = 30^0$. Solid line: Our results for horizontal polarization; Plus sign: Results for horizontal polarization in (Rothwell, 2007); Dashed line: Our results for vertical polarization; Circle: Results for vertical polarization in (Rothwell, 2007).

include any impulsive component with the amplitude of R_H^∞ or R_V^∞ . The large scale on the vertical axis may be disconcerting at first look, but it should be noted that these reflection coefficients will be convolved with incident pulses with durations on the order of nanoseconds.

Figure 3 (b) compares the reduced reflection coefficients of a Martian soil stimulant found using our technique to the results in (Rothwell, 2007). Our results agree with those in (Rothwell, 2007) very well. Since the static and optical permittivities for the soil are comparable, the relaxation effect is less dramatic than that for water while the durations of transient reflection coefficients are longer than that for water due to the longer relaxation time.

Figure 3 (c) shows the reduced reflection coefficients of a Lanthanum modified $PbTiO_3$ ferroelectric ceramic. There is an excellent agreement between our results and those in (Rothwell, 2007). The static and optical permittivities are much larger than those in the above two cases, but relaxation time is also quite large, making the durations of these reflection coefficients have the order of several nanoseconds.

Consider a Gaussian waveform incident upon a water half-space at $\theta = 30^0$. The incident field is horizontally polarized and has an amplitude of 1 V/m and a pulse width of 1 ps. The reflected waveform can be determined using the convolution,

$$E_H^r(t) = R_H(t) * E^i(t) = \bar{R}_H(t) * E^i(t) + R_H^\infty E^i(t), \tag{35}$$

where $\bar{R}_H(t)$ is shown in Figure 3 and R_H^∞ is given by (31). The reflected waveform is plotted in Figure 4, from which it is seen that the incident Gaussian waveform is maintained, but with a long tail contributed by the waveform of $\bar{R}_H(t)$ due to the relaxation effect.

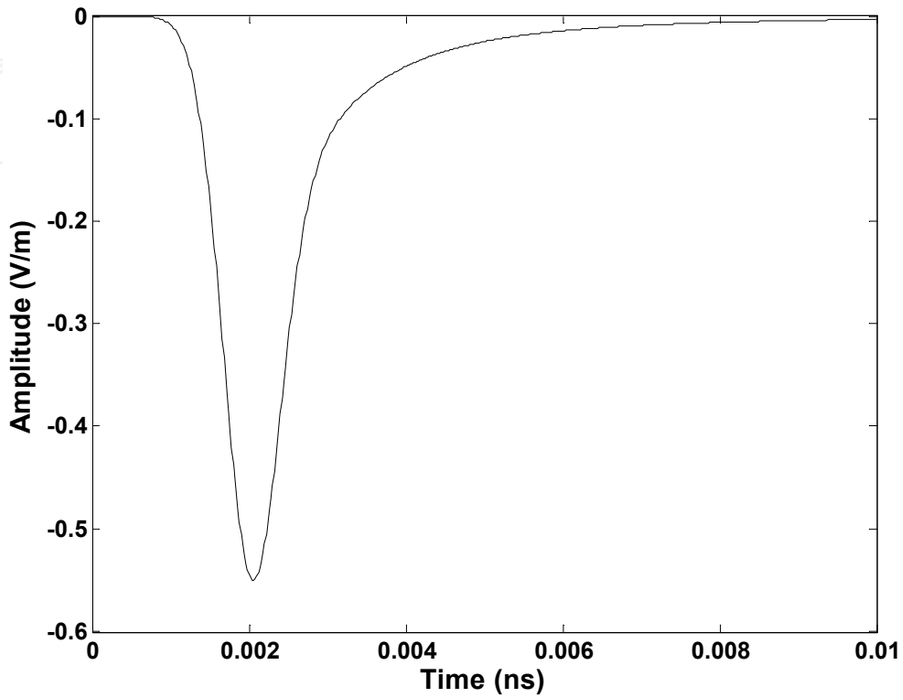

Fig. 4. Reflected waveform for a horizontally polarized Gaussian pulse incident on a water half space at $\theta = 30^0$.

4.2 Waveform parameter estimation and material characterization

Based on the above transient analysis, this technique can be utilized for the estimation of waveform parameters of reflected pulses. As an example, consider a mixture of water and ethanol with a volume fraction v_F. Here, $v_F = 0$ corresponds to pure ethanol while $v_F = 1$ corresponds to pure water. Bao et al. have shown the permittivity of this mixture is described quite well by the Debye model and have measured the Debye parameters for various volume fractions (Bao et al., 1996). The parameters can be approximated by the following expressions:

$$\varepsilon_\infty = -19.1\, v_F^2 + 18.5\, v_F + 4.8, \tag{36}$$

$$\varepsilon_s - \varepsilon_\infty = 53\, v_F + 22, \tag{37}$$

$$\tau = 0.15 \times 10^{-1.27\, vF} \text{ ns}. \tag{38}$$

For water the Cole–Cole parameter α is only 0.02, indicating that a Debye description is sufficient. However, not all polar materials have a permittivity that follows the Debye model

as closely as water. Some oil has a Cole–Cole parameter α up to 0.23 (Rothwell & Cloud, 2001). In this work, assuming that the permittivity of the mixture above is described by the Debye and Cole–Cole equations, waveform parameters estimation and material diagnosis are explored, respectively, and the corresponding results in two cases are compared with each other.

One of the most important waveform parameters is the correlation between two waveforms. It indicates the degree to which two waveforms resemble and is defined by

$$C(t) = \left(\frac{\int_0^\infty s_1(t')\, s_2(t+t')\, dt'}{s_m} \right)^2, \tag{39}$$

$$s_m = \max\left(\int_0^\infty s_1{}^2(t')\, dt', \int_0^\infty s_2{}^2(t')\, dt' \right). \tag{40}$$

Let $s_1(t)$ and $s_2(t)$ be the incident and reflected waveforms, respectively, and consider the Guassian waveform in Section 4.1 incident upon a mixture half space. The maximum value $C_{\max}$ of $C(t)$ is plotted versus the volume fraction v_F for three values of Cole–Cole parameter α and three incident angles in Figure 5 (a), and versus α for two v_F values and three incident angles in Figure 5 (b). It is seen that $C_{\max}$ increases with the increase of v_F, α and θ. Assume that a mixture with $\alpha = 0$ and $v_F = 0.7$ is desired. Whether this fraction has been achieved could be determined by examining the maximum correlation between two reflected or reduced reflected waveforms for the desired volume fraction and for the mixture to be determined Let $s_1(t)$ and $s_2(t)$ be two reflected waveforms for the desired volume fraction and for the mixture, respectively, and also let $s_1(t)$ and $s_2(t)$ be two reduced reflected waveforms for the desired volume fraction and for the mixture, respectively. $C_{\max} = 1$ indicates that the mixture has the desired volume fraction, while $C_{\max} < 1$ means that the mixture has a different volume fraction from the desired one. Using a reduced reflected waveform obtained from $\overline{E}_H^r(t) = \overline{R}_H(t) * E^i(t)$ leads to a much higher detection accuracy than using a reflected waveform calculated by $E_H^r(t) = R_H(t) * E^i(t)$. Figure 6 (a) shows that it is not easy to detect the desired mixture because $C_{\max}$ calculated using reflected waveforms does not decrease quickly in the proximity of the peak. Moreover, increasing the incident angle will significantly deteriorate the detection accuracy. The peak nearly cannot be detected for larger incident angles. In contrast, Figure 6 (b) shows that the desired mixture can be easily identified since $C_{\max}$ calculated using reduced reflected waveforms decreases sharply on two sides of the peak. Furthermore, increasing the incident angle even up to 89^0 (almost grazing incidence) will not deteriorate the detection accuracy.

Assume that a mixture with $\alpha = 0.1495$ and $v_F = 0.6$ is desired. With the range of $C_{\max}$, Figure 7 (a) indicates that it is almost impossible to detect the desired mixture because $C_{\max}$ calculated using reflected waveforms does not significantly decrease on two sides of the peak. In addition, increasing the incident angle will further deteriorate the detection accuracy. Figure 7 (b) demonstrates that the desired mixture can be identified since $C_{\max}$ calculated using reduced reflected waveforms decreases on two sides of the peak. Meanwhile, increasing the incident angle even up to 89^0 will not deteriorate the detection accuracy basically. Comparing Figure 7 (b) with Figure 6 (b), it is seen that detection of a

mixture with a desired α value is much more difficult than detection of a mixture with a desired v_F value.

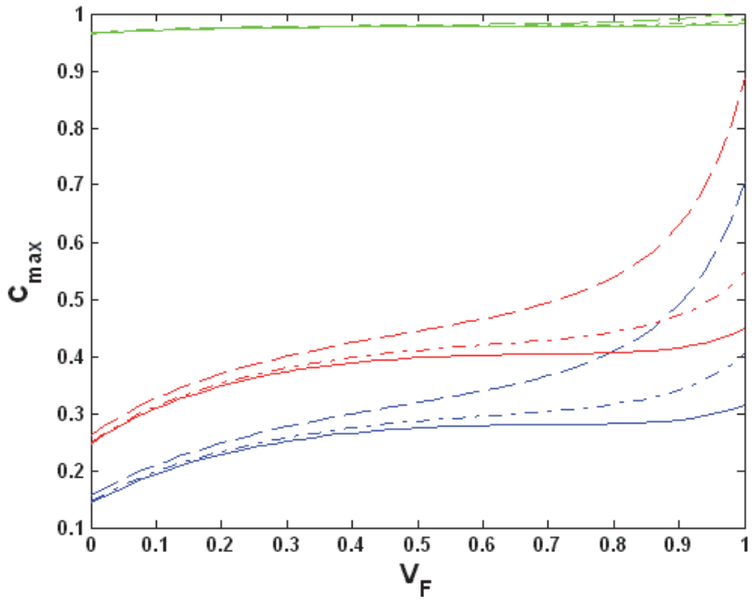

(a)

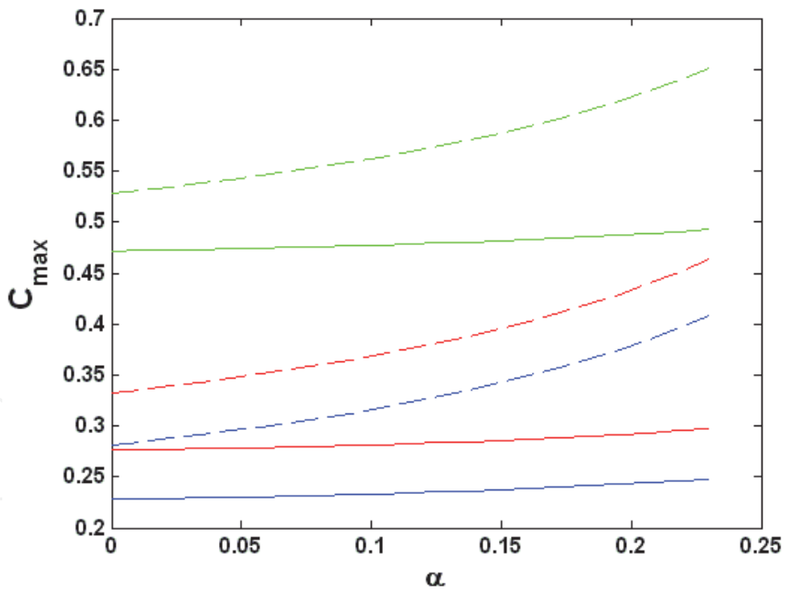

(b)

Fig. 5. Maximum correlation between the incident and reflected waveforms for a mixture irradiated by a horizontally polarized Gaussian pulse.

a. versus v_F for $\alpha = 0$ (solid lines), 0.1 (dash-dot lines) and 0.23 (dashed lines), and for $\theta = 0^0$ (blue lines), 45^0 (red lines) and 89^0 (green lines).

versus α ($0 \le \alpha \le 0.23$) for $v_F = 0.2$ (solid lines) and 0.8 (dashed lines), and for $\theta = 0^0$ (blue lines), 30^0 (red lines) and 60^0 (green lines).

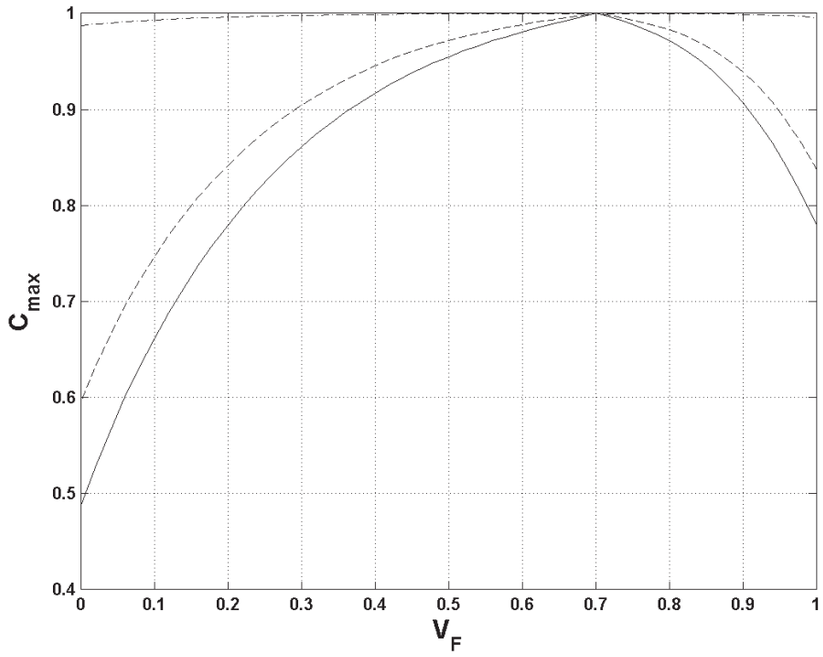

(a)

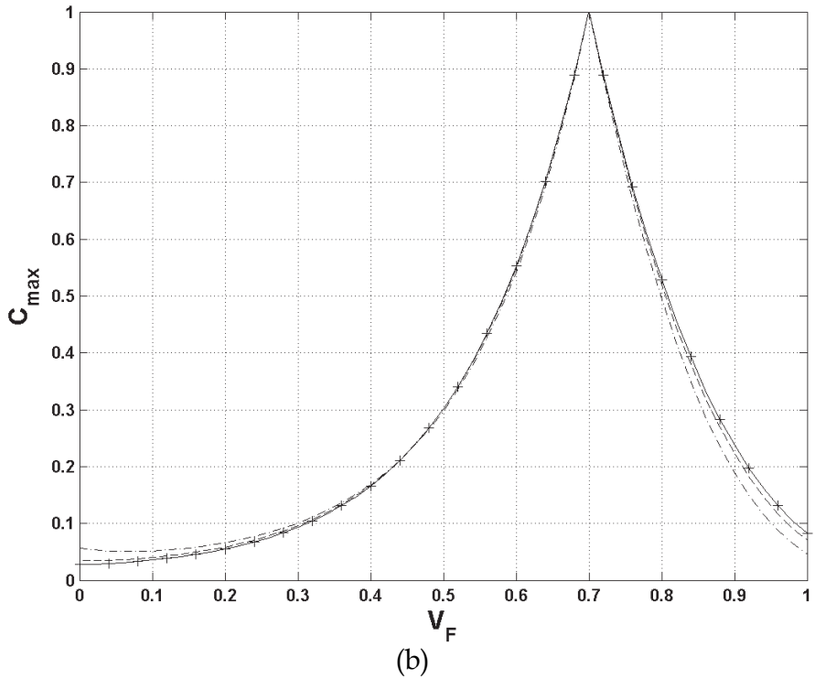

(b)

Fig. 6. Maximum correlation between two reflected waveforms (a) and between two reduced reflected waveforms (b) for the desired volume fraction and for the mixture to be determined, with a horizontally polarized Gaussian pulse incident on the mixture at $\theta = 0^0$ (solid lines), 45^0 (dashed lines) and 89^0 (dash-dot lines), when $\alpha = 0$ and v_F varying. Plus sign: Corresponding results in (Rothwell, 2007).

5. Conclusion

In general, two approaches are employed to analyze transient reflection and propagation. One is to approximate an arbitrary incident signal with a finite number of attenuating exponential signals using Prony's method and to apply numerical inversion of Laplace

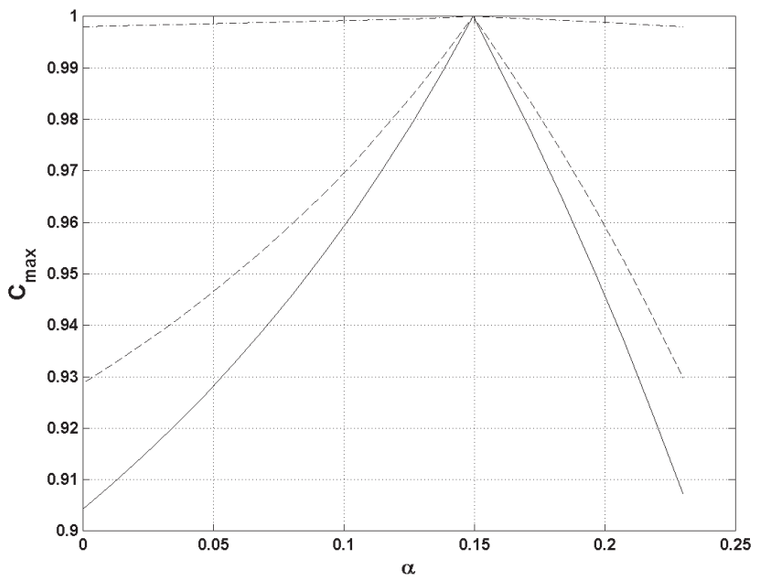

(a)

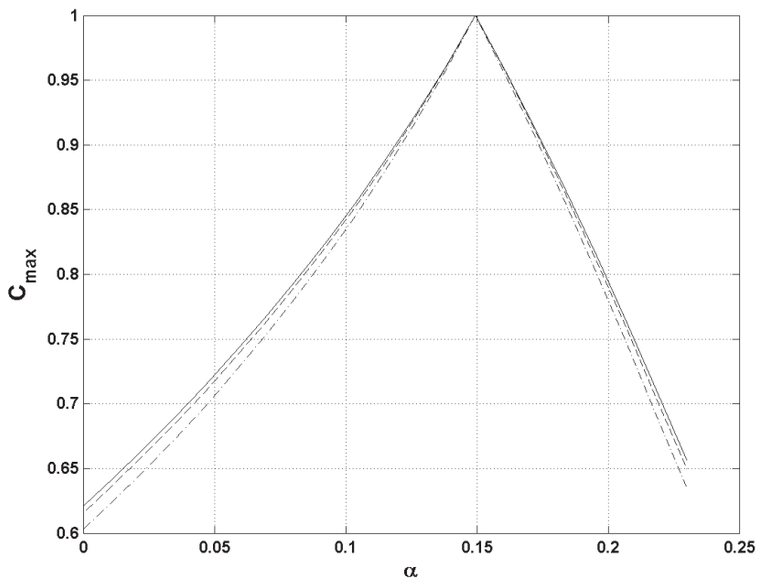

(b)

Fig. 7. Maximum correlation between two reflected waveforms (a) or between two reduced reflected waveforms (b) for the desired volume fraction and for the mixture to be determined, with a horizontally polarized Gaussian pulse incident on the mixture at $\theta = 0^0$ (solid lines), 45^0 (dashed lines) and 89^0 (green lines), when $v_F = 6$ and α varying.

transform (NILT) to the final image function, which is the product of the frequency domain reflection or tramsimission coefficient and the image function of the approximating incident signal. The accuracy of this approach is limited by the numerical errors from both NILT and the decomposition of the original incident signal into of a series of finite attenuating exponential signals (Zeng & Delisle, 2006). As shown in sections 4.1 and 4.2, another approach is to use NILT for determinating the transient reflection or transmission coefficient and to convolve the incident signal with the time domain reflection or transmission coefficient. The accuracy of this approach depends on both NILT and numerical convolution, which normally incurs smaller errors than decomposing an arbitrary signal into a series of finite attenuating exponential signals. Section 4.1 presents time domain reflection coefficients for both TE- and TM-polarized plane waves incident on a Lorentz medium half space using NILT. Three possible cases are discussed, each of which is determined by a different relationship between the damping coefficient, oscillation and plasma frequencies. The result is an exponentially damped waveform that oscillates based on the conditions of each case.

In section 4.2, the properties of a half space are described in frequency domain by the Debye and Cole–Cole models, respectively, which are commonly used to capture the relaxation-based dispersive properties. First, transient reflected pulses are analyzed and waveform parameters are estimated. Then, based on the estimation, the relationships between the waveform parameters of reflected pulses and the properties of dispersive material as well as incident angles are discussed. Meanwhile, the results obtained with the Debye model are compared to those obtained with the Cole–Cole model. The application of these results to material characterization and diagnosis is explored. It is shown that using the reduced time domain reflection coefficients often brings more physical insights and leads to an efficient algorithm and a robust scheme for dispersive material diagnosis. There is excellent agreement between our results and those in (Rothwell, 2007), which validates the correctness and effectiveness of this work.

6. References

Bao, J.-Z.; Swicord, M. & Dawes, C. (1996). Microwave dielectric characterization of binary mixtures of water, methanol and ethanol. *J. Chem. Phys.*, Vol. 104, 1996, pp. 4441-4450.

Cole, K. & Cole, R. (1941). Dispersion and absorption in dielectrics. *J. Chemical Phys.*, Vol. 9, No. 4, Apr. 1941, pp.341–351.

Cossmann, S.; Rothwell, E. & Kempel, L. (2006). Transient reflection of TE-polarized plane waves from a Lorentz-medium half-space. *J. Opt. Soc. Am., Series A*, Vol. 23, No. 9, September 2006, pp. 2320-2323.

Cossmann, S.; Rothwell, E. & Kempel, L. (2007). Transient reflection of TM-polarized plane waves from a Lorentz-medium half-space. *J. Opt. Soc. Am., Series A*, Vol. 24, No. 3, March 2007, pp. 882-887.

Debye, P. (1945). *Polar Molecules*. Dover Publications, New York, USA.

Gray, K. (1980). The reflected impulse response of a Lorentz medium. *Proc. IEEE*, Vol. 68, 1980, pp. 408-409.

Guerra J. & Eiras, J. (2004) High frequency dielectric relaxation in Lanthanum modified $PbTiO_3$ ferroelectric ceramics. *Material Res.*, Vol. 7, 2004, pp. 325–328.

Hosono, T. (1981). Numerical inversion of Laplace transform and some applications to wave optics. *Radio Sci.,* Vol. 16, No. 6, Nov.–Dec. 1981, pp. 1015–1019.

Jones, S.; Mace, R. & Or, D. (2005). A time domain reflectometry coaxial cell for manipulation and monitoring of water content and electrical conductivity in variably saturated porous media. *Vadose Zone J.*, Vol. 4, 2005, pp. 977-982.

Kosmas, P.; Rappaport, C. & Bishop, E. (2004). Modeling with the FDTD method for microwave breast cancer detection. *IEEE Trans. Microwave Theory Tech.*, Vol. 52, No. 8, Suppl. 2, August 2004, pp. 1890-1897.

Ogunsola, A.; Reggiani, U. & Sandrolini, L. (2006). Modelling shielding properties of concrete. *Proc. 17th International Symposium on Electromagnetic Compatibility*, Zurich, Switzerland, Feb. 27–March 3, 2006, pp. 34–37.

Ong, K.; Dreschel, W. & Grimes, C. (2003). Detection of human respiration using square-wave modulated electromagnetic impulses. *Microwave Optical Technol. Lett.*, Vol. 36, 2003, pp. 339- 349.

Oswald, B.; Erni, D.; Benedickter, H.; Bächtold, W. & Flühler, H. (1998). Dielectric properties of natural materials. *Proc. IEEE Antennas and Propagation Society International Symposium*, Vol. 4, 1998, pp. 2002-2005.

Oughstun, K. & Sherman, G. (1988). Propagation of electromagnetic pulses in a linear dispersive medium with aborption (the Lorentz medium). *J. Opt. Soc. Am., Series B,* Vol. 5, 1988, pp. 817-849.

Oughstun, K. & Sherman, G. (1989). Uniform asymptotic description of electromagnetic pulse propagation in a linear dispersive medium with aborption (the Lorentz medium). *J. Opt. Soc. Am., Series A,* Vol. 6, 1989, pp. 1394-1420.

Oughstun, K. & Sherman, G. (1990). Uniform asymptotic description of ultrashort rectangular optical pulse propagation in a linear, causally dispersive medium, *Phys. Rev. A*, Vol. 41, 1990, pp. 6090-6113.

Piesiewicz, R. & et al. (2005). Terahertz characterisation of building materials. *Electron. Lett.*, Vol. 41, 2005, pp. 1002-1004.

Rothwell, E. & Cloud, M. (2001). *Electromagnetics,* Chapter 4, pp. 189-348, CRC Press, Boca Raton, FL, USA.

Rothwell, E. (2007). Plane-wave impulse response of a Debye half space. *Electromagnetics*, Vol. 27, No. 4, May 2007, pp. 195–206.

Sommerfeld, A. (1914). Über die Fortpflanzung des Lichtes in dispergierenden Medien. *Ann. Phys.,* Vol. 44, 1914, pp. 177-202.

Stanic, B.; Milanovic, D. & Cvetic, J. (1991). Pulse reflection from a lossy Lorentz medium half-space (TM polarization), *J. Phys. D: Appl. Phys.*, Vol. 24, 1991, pp. 1245-1249.

Zeng, Q. (2010). *Transient Analysis of Electromagnetic Waves Based on Numerical Inversion of Laplace Transform,* Ph.D. dissertation, University of Ottawa, Ottawa, Ontario, Canada, May 2010.

Zeng, Q. & Delisle, G. (2006). Characterization for ultra wideband pulses transmitting through a lossy dielectric slab. *2006 IEEE International Conference on Ultra-Wideband (ICUWB 2006)*, Waltham, Massachusetts, USA, September 24-27, 2006, pp.213-218.

Zhang, J. & et al. (2003). Reconstruction of the parameters of Debye and Lorentzian dispersive media using a genetic algorithm. *Proc. IEEE Electromagnetic Compatibility International Symposium*, Atlanta, Georgia, USA, June 21–26, 2003, pp. 898–903.

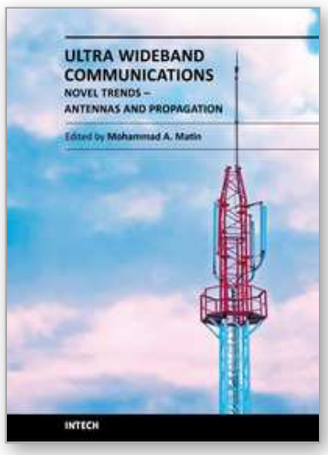

Ultra Wideband Communications: Novel Trends - Antennas and Propagation

Edited by Dr. Mohammad Matin

ISBN 978-953-307-452-8
Hard cover, 384 pages
Publisher InTech
Published online 09, August, 2011
Published in print edition August, 2011

This book explores both the state-of-the-art and the latest achievements in UWB antennas and propagation. It has taken a theoretical and experimental approach to some extent, which is more useful to the reader. The book highlights the unique design issues which put the reader in good pace to be able to understand more advanced research.

How to reference

In order to correctly reference this scholarly work, feel free to copy and paste the following:

Qingsheng Zeng and Gilles Y. Delisle (2011). Ultra Wideband (UWB) Pulse Reflection from a Dispersive Medium Half Space, Ultra Wideband Communications: Novel Trends - Antennas and Propagation, Dr. Mohammad Matin (Ed.), ISBN: 978-953-307-452-8, InTech, Available from: http://www.intechopen.com/books/ultra-wideband-communications-novel-trends-antennas-and-propagation/ultra-wideband-uwb-pulse-reflection-from-a-dispersive-medium-half-space

INTECH
open science | open minds

InTech Europe
University Campus STeP Ri
Slavka Krautzeka 83/A
51000 Rijeka, Croatia
Phone: +385 (51) 770 447
Fax: +385 (51) 686 166
www.intechopen.com

InTech China
Unit 405, Office Block, Hotel Equatorial Shanghai
No.65, Yan An Road (West), Shanghai, 200040, China
中国上海市延安西路65号上海国际贵都大饭店办公楼405单元
Phone: +86-21-62489820
Fax: +86-21-62489821

IntechOpen